

RADIO INTERFEROMETRY AT X BAND

Arthur Martirosyan Compas Professor Aaron Parsons

April 9, 2019

Abstract

We observe the Omega Nebula and the Sun with a two antenna X-Band Interferometer. Using point source fringe amplitudes at a known declination we determine the North-South baseline separation distance between our antenna to be $.750 \text{ m} \pm 0.005 \text{ m}$, and the East-West baseline to be $13.745 \text{ m} \pm 0.001 \text{ m}$. We compute the angular radius of the Sun and find its value to be 0.297 degrees.

1 Introduction

Interferometers allow us to produce information by collecting signals from different points and mixing them together and analyzing the result. A major benefit to interferometers is that by extending the separation distance between the sensors we can increase the effective size of the interferometer. As we increase the separation distance, or baseline, the collecting power increases linearly with the number of telescopes, while the angular resolution increases geometrically.

We successfully observe two targets with the interferometers on the roof of New Campbell Hall, University of California, Berkeley. We cover the configuration of the signal chain in §2.1 and a brief overview of the relevant mathematics in §2.3. We observe a point source in §3 and use the data to classify certain parameters of our interferometer. We observe one resolved source in §4 and compute its radius. Finally in §5 we discuss the implications of our findings.

2 Methods

2.1 Hardware

On the roof of New Campbell Hall are two X-Band antenna housed in dishes about 1 meter in diameter, separated as far apart as possible on the roof, approximately 15 meters. The incoming signal is routed to the 5th floor undergraduate radio astronomy laboratory, and into various components. The incoming signal has frequency = 10.7 GHz, and is brought to base-band by the various mixers and local oscillators detailed in Table 4 and figure 10.

2.2 Software

The output of the signal chain feeds into a digital multimeter, which we can access via `ugradio.HPM()`. The interferometer can be directed using `ugradio.interf`. To obtain horizon to horizon time series signal data we wrote, with the help of Professor Parsons, the script `observation_pointing.py`, which can be used to point at the Moon, the Sun, or other sources. The default settings for the script re-points the interferometer every 5 seconds. To maintain redundancy we wrote another script to only collect data called `aquisition.py`. This instructs the multimeter to record data every 1 second, saving data every 5 seconds. New pointing coordinates are calculated on the fly, for whatever the current time is. We used `ugradio.presses` to convert our coordinates to JD2019. We also used `ugradio` to calculate alt and az based on ra and dec. Various other functions and scripts were created to support the observation function, for loading and saving of data, and other tasks.

2.3 Theory

A basic layout of a two antenna interferometer is shown in Figure 1. The time delay that the separation induces is

$$\tau_{tot} = \tau_g(\alpha^\circ) + \tau_c \quad (1)$$

where $\alpha^\circ = \text{hourangle}$, τ_g is the geometric delay, and τ_c is the physical cable delay caused by the different length cables. The signals that are received by the two antenna oscillate based on the frequency ν .

$$E_1(t) = \cos(2\pi\nu t) E_2(t) = \cos(2\pi\nu[t + \tau_{tot}]) \quad (2)$$

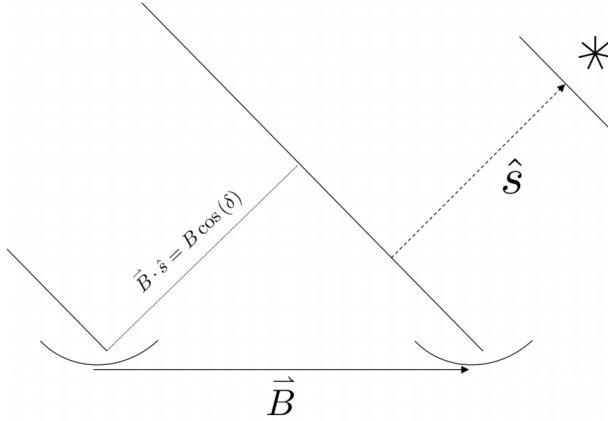


Figure 1: Geometry of a two antenna interferometer. The two dishes are the antenna, the solid vector pointing towards the star is the unit vector \hat{s} . The long solid lines are plane waves emanating from the source, while the dash line represents the geometric separation distance between the antenna. The source is considered to be so far away that the unit vector that points towards it is the same for both antenna. Plane waves from the source strike one antenna before the other, introducing a time delay.

The interferometer signal chain multiplies these two signals together. After some light trigonometry and dropping of terms that average to zero, we arrive at the fringe amplitudes

$$F(\alpha^\circ) = \cos(2\pi v[\tau_g l + \tau_c l]) \quad (3)$$

which easily expands into

$$F(\alpha^\circ) = \cos(2\pi v\tau_c l)\cos(2\pi v\tau_g l) - \sin(2\pi v\tau_c l)\sin(2\pi v\tau_g l) \quad (4)$$

Equation 4 represents the fringe amplitudes we expect to read with our multimeter when we make our observations. The corresponding fringe frequencies f_f are laid out in equation 26, and are also a function of (α°) .

3 Point Source

3.1 Omega Nebula Observation

The Omega Nebula is a region of star formation approximately 6000 lightyears away [1] and is one of the largest star-forming regions in the Milky Way galaxy. It has coordinates $(\alpha, \beta)_{2000} = (275.11^\circ, -16.17667^\circ)$. We observe the Omega Nebula for 5 hours on March 10, 2019, sampling the fringe amplitude every second. The large number of samples allows us to fit a high order polynomial to the data without fear of over fitting. We subtract this fit from the data to force the data closer to be closer to theory. The time data for our observations can be viewed in table 2.

3.2 Omega Nebula Fringe Frequencies

Our time series data consists of just over 17 000 fringe amplitudes. To find the fringe frequencies hidden in the data we will compute multiple power spectra. If we have time series data with of a

signal that oscillates at a steadily changing frequency f_f we can compute the power spectrum of many different windows in the data and should see peaks at the frequencies f_f .

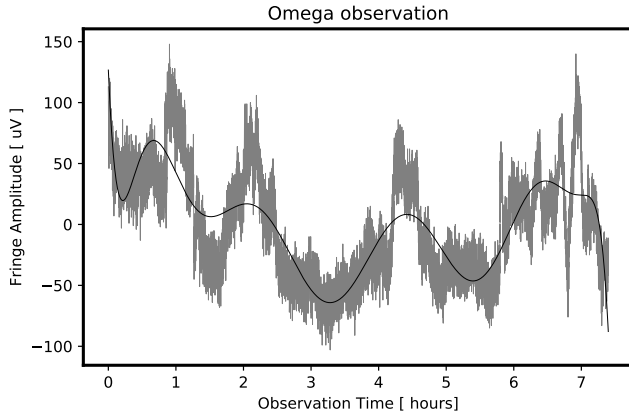


Figure 2: Fringe amplitudes collected during a 10 hour observation of the omega Nebula, with a 12th degree polynomial fitted to the data. We subtract the mean of the data to eliminate a DC offset introduced by our equipment

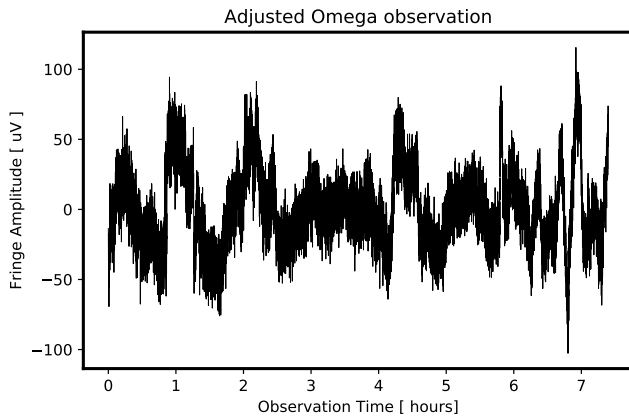


Figure 3: Omega Nebula observation fringe amplitudes minus a 10th degree polynomial fit. The adjustment was relatively successful

In Figure 4, the 'Eye Of Sauron', we present 36000 spectra. Each row represents a power spectrum calculated using a 1200 second window. We compute a spectrum for a window, then increment the window start time by one second, and compute a new spectrum. It is clear from the figure that we have not successfully eliminated the DC offset, as a dark line showing high power is visible at 0 Hz. Though difficult to make out, there are also arcing lines of strong power that are our fringe frequencies f_f . As predicted, they begin at a low frequency at the start of the observation and increase until the source is overhead, then decrease until the end of the observation

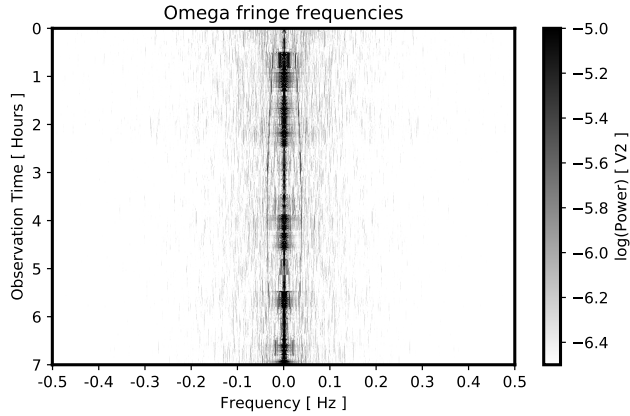


Figure 4: 36 000 separate power spectra, each representing a 1200 second window. By using a large window and incrementing the starting position of each window by one second we produce a large number high resolution power spectra. The dark line at 0 Hz is our unsuccessfully eliminated DC offset. The lines that arc from 0 Hz to 0.05 Hz and back are our fringe frequencies ff .

3.3 Interferometer Calibration

Now that we are certain that we observed our target point source, and assuming that we take the coordinates of the target to be exact and fixed quantities, we can compute various parameters for our interferometer. The fringe amplitude for a point source can be found by rewriting equation 4

$$F(\alpha^\circ) = A\cos(2\pi\xi) + B\sin((2\pi\xi)) \quad (5)$$

where A and B are unknown coefficients. Unless the source is directly ahead, the plane waves coming from our point source strike the nearer antenna first, causing one signal to be intercepted before the other. This time delay corresponds to the antenna separation distances, and is embedded in ξ .

$$\xi = \left[\frac{B_{ew}}{\lambda} \cos \delta \right] \sin \alpha^\circ + \left[\frac{B_{ns}}{\lambda} \sin L \cos \delta \right] \cos \alpha^\circ \quad (6)$$

Here, B_{ew} is the East-West separation of the antennas, while B_{ns} is the North-West separation, and L is the latitude of the interferometer. To simplify ξ we define two dimensionless quantities which are functions of the baselines:

$$Q_{ew} = \left[\frac{B_{ew}}{\lambda} \cos \delta \right] \quad \& \quad Q_{ns} = \left[\frac{B_{ns}}{\lambda} \sin L \cos \delta \right] \quad (7)$$

$$\xi = Q_{ew}\sin(\alpha^\circ) + Q_{ns}\cos(\alpha^\circ) \quad (8)$$

3.4 Brute Force Least Squares

We fit Equation 5 to the fringe amplitudes in Figure 3 to determine the baseline distances, which are now embedded in the Q values. We guess a pair of Q values and then perform a standard least squares fit for the unknown coefficients A and B. Using matrices this is a speedy process. We define the $m \times 1$ column vector of the measured fringe amplitudes \vec{b} , the 2×1 column vector of the unknown coefficients

$$\vec{x} = \begin{bmatrix} A \\ B \end{bmatrix} \quad (9)$$

and the $m \times 2$ matrix of the trigonometric terms

$$\mathbf{M} = [\cos(2\pi\xi) \quad \sin(2\pi\xi)] \quad (10)$$

The $m \times 1$ column vector of the fitted fringe amplitudes \vec{y} is found via simple linear algebra

$$\mathbf{M}\vec{x} = \vec{b} \quad (11)$$

$$\vec{x} = (\mathbf{M}^\top \mathbf{M})^{-1} \mathbf{M}^\top \vec{b} \quad (12)$$

$$\vec{y} = \mathbf{M}\vec{x} \quad (13)$$

For each fit we compute the sum of the squares of the residuals, S^2 :

$$S^2 = \frac{1}{m-2} \sum_{i=1}^m (b_i - y_i)^2 \quad (14)$$

We store the value and then guess a new pair of Q values to recompute S^2 .

3.4.1 Baselines

Using the minimum Q values found with Figure 5, we solve for the baselines in Equation 7 to find

$$B_{ew} = 13.745m \quad (15)$$

$$B_{ns} = 0.750m \quad (16)$$

3.4.2 Baseline Uncertainties

The baseline values are computed using found values of Q, so to find the error on the baseline we must first find the errors on Q. Fortunately this is not too difficult. At its minimum, the grid of S^2 values has a curvature that can be defined by a matrix of second partial derivatives

$$\mathbf{H} = \begin{bmatrix} \frac{1}{2} \frac{\partial^2 S^2}{\partial Q_{ew}^2} & \frac{\partial^2 S^2}{\partial Q_{ew} \partial Q_{ns}} \\ \frac{\partial^2 S^2}{\partial Q_{ew} \partial Q_{ns}} & \frac{1}{2} \frac{\partial^2 S^2}{\partial Q_{ns}^2} \end{bmatrix}. \quad (17)$$

To compute these partial derivatives we make use of numpy.diff(), iterating through the grid of S^2 in the appropriate directions. The inverse of \mathbf{H} is the covariance matrix for Q_{ew} and Q_{ns} , and the diagonal terms represent their error. With these errors for the Q values we can compute the uncertainties on the baseline measurements with standard error propagation techniques.

$$\sigma_{B_{ns}} = 0.005m \quad (18)$$

$$\sigma_{B_{ew}} = 0.001m \quad (19)$$

3.5 Omega Nebula Fringe Frequencies

Having classified our interferometer, we compare the difficult to see fringe frequencies in Figure 4 to theoretical values. The theoretical values can be found with

$$f_{f, \text{theory}} = Q_{ew} \cos(\alpha^\circ) + Q_{ns} \sin(\alpha^\circ) \quad (20)$$

We must extract the observed fringe frequencies from the power spectra in Figure 4. We create a function that takes in an array and a threshold value. It iterates through the array, comparing elements with their neighbors and with the threshold. When a value is larger than the threshold and larger than all its neighbors, we save that value as a peak. For the Omega Nebula observation we expect two or three peaks for each spectra, two for the actual f_f we desire and a third for the strong DC offset we were unable to eliminate. For each spectrum, we set the threshold at the spectrum's maximum value, and repeatedly lower the value until the desired number of peaks are found. The located fringe frequencies are shown in Figure 5.

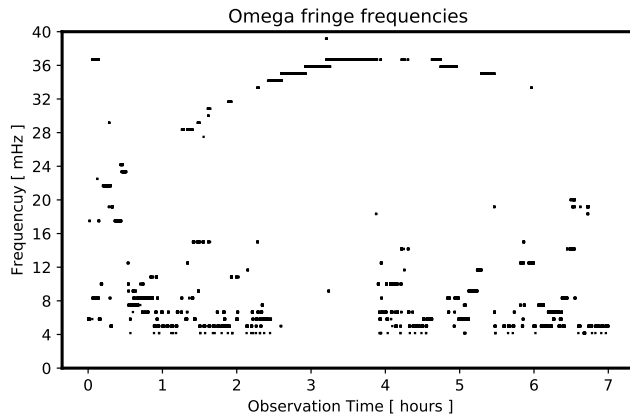


Figure 5: Omega Nebula fringe frequencies. The noisy data, the boxes, were found by applying a peak finder algorithm to the power spectra from Figure 4

4 Resolved Objects

For the resolvable objects, their right ascension and declination values change quickly. Our observing function takes this into account, recomputing these coordinates before finding the altitude and azimuth of the targets.

4.1 Observations

4.1.1 The Sun

The brightest object in our sky, and one that emits strongly in the X-Band, the Sun makes an excellent target object. We observe the Sun for 2 hours, sampling the fringe amplitude every second. In Figure 6 we can see the fringe amplitudes being multiplied by some modulating function.

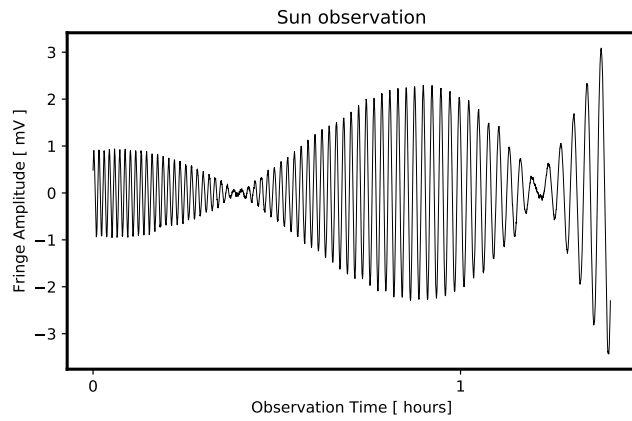


Figure 6: Fringe amplitudes collected during a 2 hour observation of the Sun. The fringe amplitudes are clearly modulated by some function that varies with hour angle, as the modulation mirrors about $\alpha = 0$. In an effort to eliminate a DC offset introduced by our equipment we subtract off the mean of the data

4.2 Fringe Frequencies

4.2.1 Solar Fringe Frequencies

For our solar time series data we compute the power spectra much like in §3.2, with one small difference. The sun fringe amplitudes wave moderate banding effects we must account. The banding is the result of oscillations that are cut off at non-integer wavelengths. The fringe frequencies are well defined in Figure 7.

We also extract the actual fringe frequencies from the spectra plot in figure 8 and compare the to the theoretical values, using the process in 3.5 and find that they match very well. The peaks found for the sun exhibit no noise, though a curious step pattern is visible.

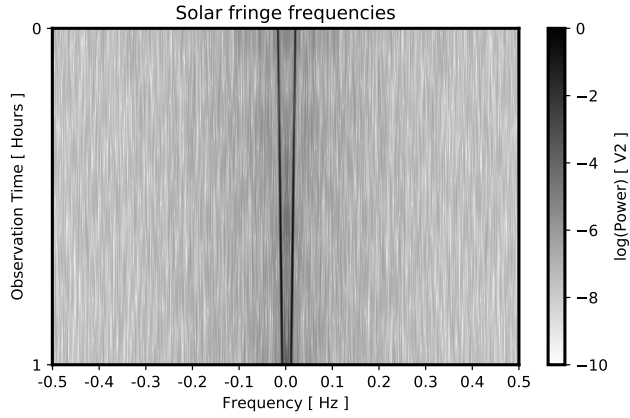


Figure 7: 36 000 spectra created from solar fringe amplitude windows, each 1200 seconds wide. As before we increment each row by one second. The DC offset is still visible, though not as strongly as in the Omega Nebula spectra.

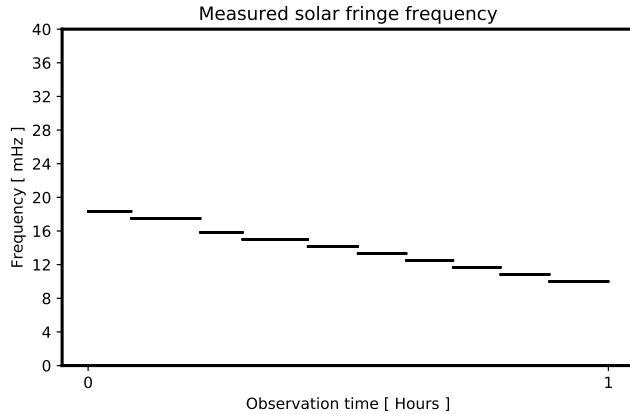


Figure 8: 36 000 fringe frequencies extracted from our power spectra data and the same number computed from theory. The data match quite well, though there is a curious quantization to the actual data

4.3 Size

In theory our resolved sources are perfectly disk shaped with even intensity across their surfaces. Our interferometers are performing a Fourier transform of the sky, and the Fourier transform of a disk is a Bessel function of the first kind. The fringe amplitude signal from perfect disk sources will be multiplied by this modulating function. A Bessel function representing these theoretical perfect disks can be written as

$$MF_{theory} \approx \delta h \sum_{n=-N}^{n=+N} \left[1 - \left(\frac{n}{N} \right)^2 \right]^{1/2} \cos \left(\frac{2\pi f_f R n}{N} \right) \quad (21)$$

In Equation 21, R is the radius of the source in radians, f_f is the fringe frequency in inverse radians, and we consider the intensity to be broken up into $2N + 1$ pieces, one for each hour angle. The Bessel function crosses zero repeatedly, and the value of its first crossing, ζ , can be used to find the radius of the disk.

$$R = \frac{\zeta}{f_f} \quad (22)$$

We expect our resolved sources to be only approximately disk shaped, due to intensity variation across the disk and irregular protuberances at the edge of the disk. For example, solar flares can project off the surface and sunspots alter the intensity. These variations away from a perfect disk mean the modulating function will not be exactly MF_{theory} .

4.3.1 Solar Radius

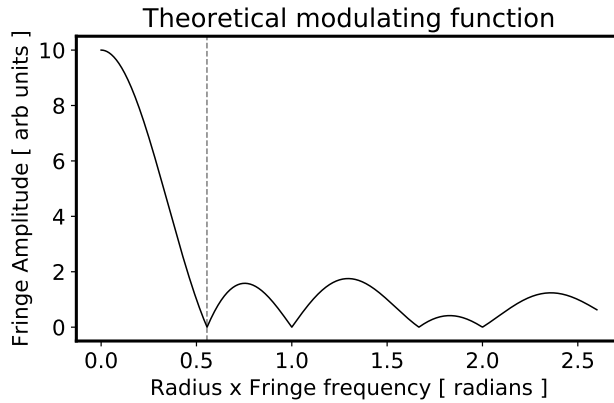


Figure 9: Theoretical modulating function with the point of the first minimum indicated. The modulating function (black) is computed with Equation 27. We find the first minimum to be at $= 0.555$. By comparing the location of this minimum with the corresponding location on the equivalent figures for our resolved sources we will be able to measure their angular radii

To determine the first minimum required for Equation 28 we review to the solar fringe amplitudes in Figure 9. The fringe amplitudes have been modulated by our some function, which we take to be similar in shape to the theoretical modulating function MF_{theory} .

We analyze the absolute value of the fringe amplitudes and find the first minimum occurs at $f_f = 118.5$ cycles/radian, so using Equation 22:

$$R_{sun} = \frac{0.615}{118.5/Radian} \quad (23)$$

$$R_{sun} = 0.005189 \text{ radians} \quad (24)$$

$$R_{sun} = 0.2967^\circ \quad (25)$$

If we consider the Sun to be a distance of 1 AU from the our interferometer, then simple geometry allows us to compute the radius of the Sun in kilometers.

$$R_{sun,km} = \sin(R_{sun}) \circ 1AU \circ \frac{149597870.7km}{AU} \quad (26)$$

$$R_{sun,km} = 774672km \quad (27)$$

When compared to the actual radius of the Sun, 695 508 km, we find our values have a 7% error.

Conclusion

In conclusion we were able to make observations of two celestial targets, the Sun and the Omega Nebulae. We then classified the physical parameters of the Interferometer on top of New Campbell Hall to find teh baseline separation to be $13.745 \text{ m} \pm 0.001 \text{ m}$ and the direct baseline separation to be $13.765\text{m} \pm 0.003\text{m}$ (table 1). We used these parameters to compute the radius of the sun as well as its distance which can be viewed in table 3, which yielded a 7% error in our calculations. This lab was greatly important in exercising curve fitting and error analysis using least square models.

Distribution of Effort

This lab heavily relied on computational work which all of us did individually. I was responsible for writing the telescope pointing script while Oscar wrote the script to gather data. Roman worked on calculating a baseline and Matthew worked on error analysis. Our appropriate code can be viewed under our corresponding branches:

<http://github.com/arthurm101/radiolab/blob/Arthur/Lab3> (28)

References

- [1] The omega nebula. <https://www.nasa.gov/feature/goddard/2017/messier-17-the-omega-nebula-or-swan-nebula/> , 2019. Online; accessed 9 April 2019.

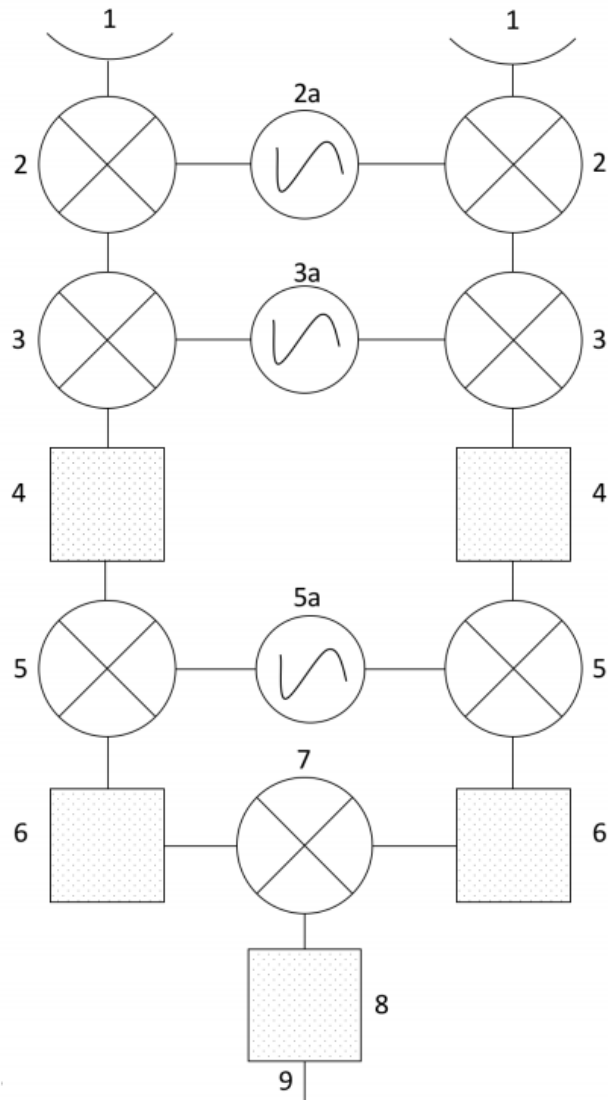


Figure 10: Signal chain diagram. For a description of the components see Table 4. X-band antennas are at the top and the signal chain output is at the bottom. The boxes with the dots are filters, while the circles with the x's inscribed are mixers. The circles with the stylized S are local oscillators.

Table 1: Interferometer parameters determined via brute force least squares fit.

	B_{ns}	B_{ew}	B_{direct}
Distance [m]	0.750 ± 0.005	13.745 ± 0.001	13.765 ± 0.003

Table 2: Start dates and times of our observations. The end time can be found using the observation duration. All samples were recorded using antennas at New Campbell Hall, University of California, Berkeley. Latitude 37.873 199° , Longitude 1° , Altitude 120 m

Target	UTC	Unix	Julian Date	Duration [seconds]
Sun	03/15/2019 4:57pm	1552694252.927677	2458558.4982977742	5068
Omega Nebulae	3/10/2019 3:43am	1552214609.558489	2458552.9468698897	17183

Table 3: Object diameters. Comparison of the first minimum of the theoretical and actual amplitude modulation functions provides the radius in radians. We convert to diameter and present the result in multiple formats

Object	Radians	Degrees	Arcseconds	Kilometers	Actual Diameter [m]	Percent Error
Sun	0.00988	0.564	2037.8	14477900	1391000	6.258

Table 4: Signal chain components describing figure below

#	Description	Frequency
1	Incoming Signal	10.7 Ghz
2	Double Sideband Mixer	-
2a	Local oscillator 1	8.75 Ghz
3	Double Sideband Mixer	-
3a	Local Oscillator 2	1.37 Ghz
4	Bandpass Filter	312 Mhz to 342 Mhz
5	Double Sideband Mixer	-
5a	Local Oscillator	327.5 Mhz
6	Low Pass Filter	-2Hz to 2Hz
7	Multiplier	-
8	Low Pass Filter	0.17 Hz
9	Output Signal	-